The Meteoritical Society

Meteoritics & Planetary Science 44, Nr 2, 159–174 (2009)
Abstract available online at http://meteoritics.org

The Puerto Lápice eucrite

Jordi LLORCA[1*], Ignasi CASANOVA[1, 2], Josep M. TRIGO-RODRÍGUEZ[3], José M. MADIEDO[4], Julia ROSZJAR[5], Addi BISCHOFF[5], Ulrich OTT[6], Ian A. FRANCHI[7], Richard C. GREENWOOD[7], Matthias LAUBENSTEIN[8]

[1]Institut de Tècniques Energètiques, Universitat Politècnica de Catalunya, Diagonal 647, ed. ETSEIB, 08028 Barcelona, Spain
[2]Centre for Research in Nanoengineering, Universitat Politècnica de Catalunya, Campus Nord B1-109C, 08034 Barcelona, Spain
[3]Institute of Space Sciences (CSIC) and Institut d'Estudis Espacials de Catalunya (IEEC), Campus UAB, Facultat de Ciències C-5p 2a planta, 08193 Bellaterra, Spain
[4]Facultad de Ciencias Experimentales, Universidad de Huelva, 21071 Huelva, Spain
[5]Institut für Planetologie, Universität Münster, Wilhelm-Klemm-Str. 10, 48149 Münster, Germany
[6]Max Planck Institut für Chemie, Becherweg 27, 55128 Mainz, Germany
[7]Planetary and Space Sciences Research Institute, The Open University, Milton Keynes, MK7 6AA, UK
[8]Laboratori Nazionali del Gran Sasso (I.N.F.N.), S.S. 17/bis km 18+910, 67010 Assergi (AQ), Italy
[*]Corresponding author. E-mail: jordi.llorca@upc.edu

(Received 24 January 2008; revision accepted 29 August 2008)

Abstract–Puerto Lápice is a new eucrite fall (Castilla-La Mancha, Spain, 10 May 2007). In this paper, we report its detailed petrography, magnetic characterization, mineral and bulk chemistry, oxygen and noble gas isotope systematics, and radionuclide data. Study of four thin sections from two different specimens reveal that the meteorite is brecciated in nature, and it contains basaltic and granulitic clasts, as well as recrystallized impact melt and breccia fragments. Shock veins are ubiquitous and show evidence of at least three different shock events. Bulk chemical analyses suggest that Puerto Lápice belongs to the main group of basaltic eucrites, although it has a significantly higher Cr content. Oxygen isotopes also confirm that the meteorite is a normal member of the HED suite. Noble gas abundances show typical patterns, with dominant cosmogenic and radiogenic contributions, and indicate an average exposure age of 19 ± 2 Ma, and a Pu-fission Xe age well within typical eucrite values. Cosmogenic radionuclides suggest a preatmospheric size of about 20–30 cm in diameter.

INTRODUCTION

The Puerto Lápice eucrite fell in Ciudad Real, Castilla-La Mancha, Spain (39°21′N, 3°31′W) on May 10, 2007, at 17 h 57 m UTC. The fireball followed a south to north trajectory and was widely seen all over Spain, with an absolute magnitude of −14 ± 4. A series of clearly audible detonations were heard at various points along its atmospheric trajectory. More details on the trajectory of this daylight bolide have been compiled by the Spanish Meteor and Fireball Network (SPMN) and are described by Trigo-Rodriguez et al. (2009). Shortly after its fall in olive groves and vineyards, approximately 70 fragments were recovered, with a total mass of about 0.5 kg. The Puerto Lápice meteorite is the 32nd recovered eucrite fall worldwide (8th in Europe), and the second meteorite fall recovered this century in Spain (Llorca et al. 2005; Trigo-Rodríguez et al. 2006).

Howardites, eucrites, and diogenites have long been recognized as representing a related group of meteorites and are therefore collectively referred to as the HED suite (Mittlefehldt et al. 1998). Based largely on reflection spectroscopy, the HED suite is thought to be derived from the asteroid 4 Vesta (Drake 2001). The NASA Dawn mission, launched successfully in September 2007, is due to arrive at Vesta in 2011 when it will commence detailed observations of the asteroid using a series of remote-sensing instruments (Russell et al. 2004). The anticipated arrival of the DAWN spacecraft has generated a renewed impetus to undertake detailed laboratory studies of HED meteorites. The Puerto Lápice eucrite, being a recent fall, is a new and comparatively pristine sample that affords a unique opportunity to directly study processes that may have operated on 4 Vesta. Here we have used a comprehensive set of analytical techniques to characterize the Puerto Lápice eucrite, including petrology, mineralogy, chemistry, magnetism, noble gas, oxygen isotope, and cosmogenic radioisotope analysis. It is important to note that recent studies indicate that not all eucritic meteorites are derived from a single parent asteroid. The

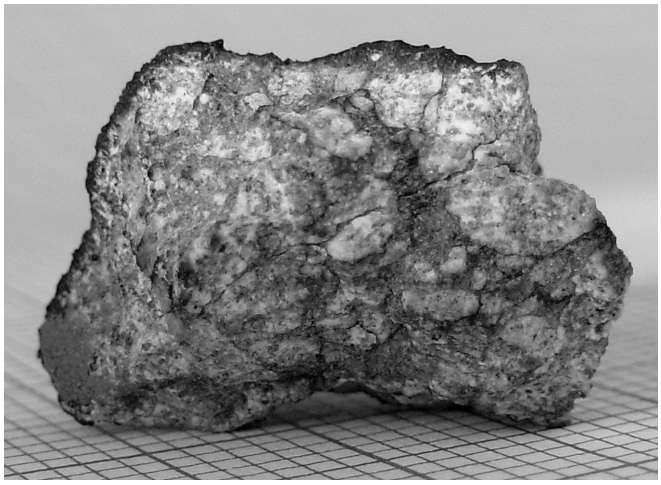

Fig. 1. Hand specimen of the Puerto Lápice eucrite as it was encountered shortly after the meteorite fall. It shows a brecciated nature (squares are 1 mm long).

oxygen isotope composition and chemistry of two meteorites originally classified as eucrites, Ibitira and NWA 011, have been determined to be very different from that of other known basaltic achondrites (Yamaguchi et al. 2002; Floss et al. 2005; Mittlefehldt 2005). This suggests that Ibitira and NWA 011 may be derived from parent asteroids other than 4 Vesta. This discovery has further stimulated interest in the study of basaltic meteorites. New eucrite samples such as Puerto Lápice must be carefully studied in order to assess whether or not they are in fact members of the HED suite.

PETROGRAPHY AND MINERAL CHEMISTRY

Four polished thin sections (LM 1 [Barcelona]; PL07206, PL07207, and PL07208 [Münster]) from two meteorite specimens were studied by optical microscopy in transmitted and reflected light (Zeiss Axiophot), scanning electron microscopy (JEOL JSM 840 electron microscopes in Barcelona and Münster), energy dispersive X-ray analysis (Oxford Instruments and Link Systems), and electron microprobe (Cameca SX-50; Barcelona).

A visual examination of the cut surfaces of various hand specimens and thin sections reveals that Puerto Lápice is brecciated in nature (Figs. 1 and 2). Petrographic study reveals the presence of different clast types, each with distinct textural features (Figs. 3 and 4). Diogenitic fragments have not been observed in the thin sections studied. The fragments are embedded in a clastic, well-consolidated matrix (Fig. 3a). Significant amounts of interstitial material representing late melts are present in a number of areas (Fig. 4f) and may have been produced during the lithification process. The formation of interstitial melt during breccia consolidation has been well-documented in other samples (e.g., Kiefer 1975; Bischoff et al. 1983; Bischoff and Stöffler 1992). A variety of different types of rock fragments are embedded within the clastic matrix and these are described in detail below.

Basaltic Eucrite Clasts

Typical examples of basaltic clasts are shown in Figs. 3b and 3c and consist of an intergrowth of pyroxene and plagioclase laths up to several hundreds of microns in length. Rarely, smaller anhedral grains of plagioclase occur embedded poikilitically in larger low-Ca pyroxene crystals. A few shock veins occur within this lithology. High-Ca pyroxenes occur as lamellae in low-Ca pyroxene hosts, although the inverse situation (low-Ca lamellae in high-Ca host) has also been observed. Ilmenite is present in minor to accessory amounts, forming grains that can reach almost 100 μm in size. Some spinel grains with TiO_2 contents of up to 16.4 wt% occur (Table 1), suggesting the presence of ulvöspinel (Fe_2TiO_4) associated with chromite. In some of the basaltic clasts there are fine-grained, recrystallized areas which display sharp contacts with the surrounding host material (lower left quadrant of Fig. 3d and Fig. 4b; right-hand side). In Fig. 3d this fine-grained lithology shows some textural layering with an outer rim of about 300 μm in width and an average grain size of less than 20 μm. Grain size increases towards the inner areas with sizes typically between 100 and 200 μm. In these fine-grained areas high-Ca pyroxenes generally occur as small, dispersed grains or exsolution lamellae of a few microns diameter enclosed within the larger orthopyroxene crystals. Ilmenite, troilite, and minor Ti-bearing chromite (up to about 3 wt% TiO_2) are present as accessory minerals. These phases are randomly distributed as anhedral grains throughout the fine-grained, recrystallized portion and can reach a few tens of microns in size. A few small grains (<20 μm) of silica have also been identified. These fine-grained recrystallized clasts also exist as individual fragments within the Puerto Lápice bulk breccia (see below).

Coarse-Grained Eucritic Fragments

Several coarse-grained eucritic fragments were encountered (Fig. 3f), with grain sizes varying from a few hundreds of microns to over 1 mm. A remarkable feature of some of these clasts is their abundance of silica and ilmenite (Fig. 4a), which is significantly higher than in the other textural types. Silica appears as anhedral grains of a few tens of microns, spatially associated with ilmenite and/or troilite (Fig. 4a). Metal is present in at least one of these coarse-grained fragments. Troilite is stoichiometric FeS and the metal (about 300 microns in size) is Ni-free, likely originated from silicate reduction. We also observed coarse-grained fragment areas with recrystallized textures similar to those found in the granulitic clasts.

Granulitic Clasts

Many large clasts in Puerto Lápice have a highly recrystallized texture (Fig. 3e), consisting of granules of

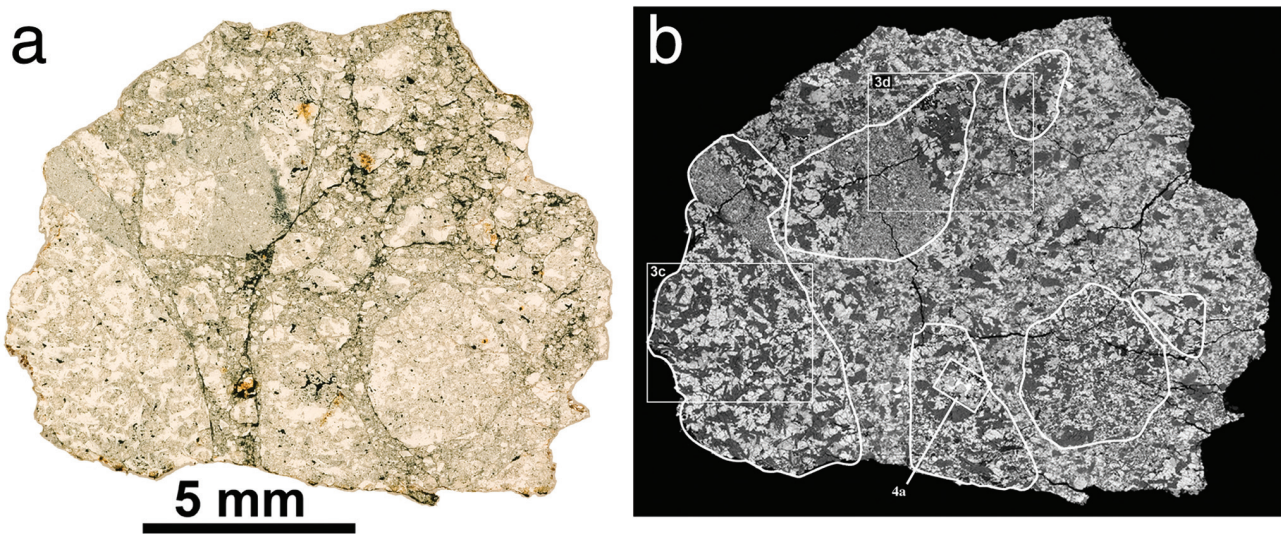

Fig. 2. Thin section picture in transmitted light (a) and back-scattered electron photomosaic image (b) of the Puerto Lápice thin section LM 1. In (b) the six largest fragments are outlined. This figure clearly shows that the fine-grained, recrystallized areas within the two largest clasts are parts of the basaltic lithology. Boxes identify details shown in Figs. 3 and 4.

pyroxene and plagioclase (50–200 μm in apparent diameter) and of minor or accessory minerals (e.g., ilmenite, chromite, SiO_2 phase). The mineral constituents have well-developed 120° triple junctions and curved boundaries (Fig. 3e). There is little indication of a remnant igneous texture. These clasts bear a striking resemblance to the Asuka-881388 granulitic eucrite breccia (Yamaguchi et al. 1997). Such highly recrystallized granulitic clasts require extensive metamorphism. Yamaguchi et al. (1997) pointed out that the most likely source of the heat for metamorphism is simple burial of a succession of lava flows as the crust grew by volcanism and intrusions.

Recrystallized Impact Melt Fragments

As described above, fine-grained, highly recrystallized areas are present within the basaltic lithology. This fine-grained lithology is also present as individual fragments within the Puerto Lápice breccia (Fig. 4c). Pyroxenes and plagioclase form anhedral grains of up to a few tens of microns, and show numerous 120° triple-point junctions. This microstructure may have formed by recrystallization of a fine-grained precursor, possibly an impact melt. The most abundant opaque phase identified within this lithology is ilmenite, which forms tiny dispersed grains of a few microns in size. These grains have a similar composition to the other ilmenites analyzed in the meteorite. Chromite is relatively abundant in this material, whereas troilite is rare.

Breccia Clasts (Breccia-in-Breccia)

A fine-grained breccia fragment, with an apparent diameter of several hundred μm has been identified within the Puerto Lápice meteorite (Fig. 4e) and consists of angular mineral clasts embedded in a fine-grained matrix (unresolvable by SEM techniques). Angular fragments of pyroxene, plagioclase, ilmenite, chromite, and an SiO_2 phase are also incorporated in this breccia fragment. Similar clasts of clastic matrix (breccia-in-breccia structure) have been found in several howardites and chondrites (e.g., Bischoff et al. 1993, 2006; Metzler et al. 1995; Pun et al. 1998). It is suggested that these clasts formed and were compacted elsewhere on the surface of the parent body and were then admixed as lithic clasts into the host breccias by impact (Bischoff et al. 2006). We suggest that the Puerto Lápice breccia clast formed in a similar manner, i.e., as a pre-existing fragmented parent body soil that was subsequently lithified. Later, due to impact processing this lithology was again fragmented and clasts of it were mixed with other eucrite lithologies prior to final consolidation of the present Puerto Lápice meteorite.

Fine-Grained, Anorthite-Normative Clast

A fine-grained clast, about 300 μm in apparent diameter has abundant tiny inclusions of Ca-rich pyroxene, FeS grains, and lumps of SiO_2-normative materials embedded in an anorthitic plagioclase-normative groundmass (Fig. 4d). This fragment is possibly a crystalline impact melt breccia.

Mineral Chemistry

Silicates are, within 1σ of molar contents of end-members, indistinguishable in composition, irrespective of their grain size or location in all clasts described above (Table 2). Low-Ca pyroxenes are $Wo_{3.0}En_{38}Fs_{59}$ and high-Ca pyroxenes $Wo_{44}En_{31}Fs_{25}$; plagioclase (An_{92}) is among the

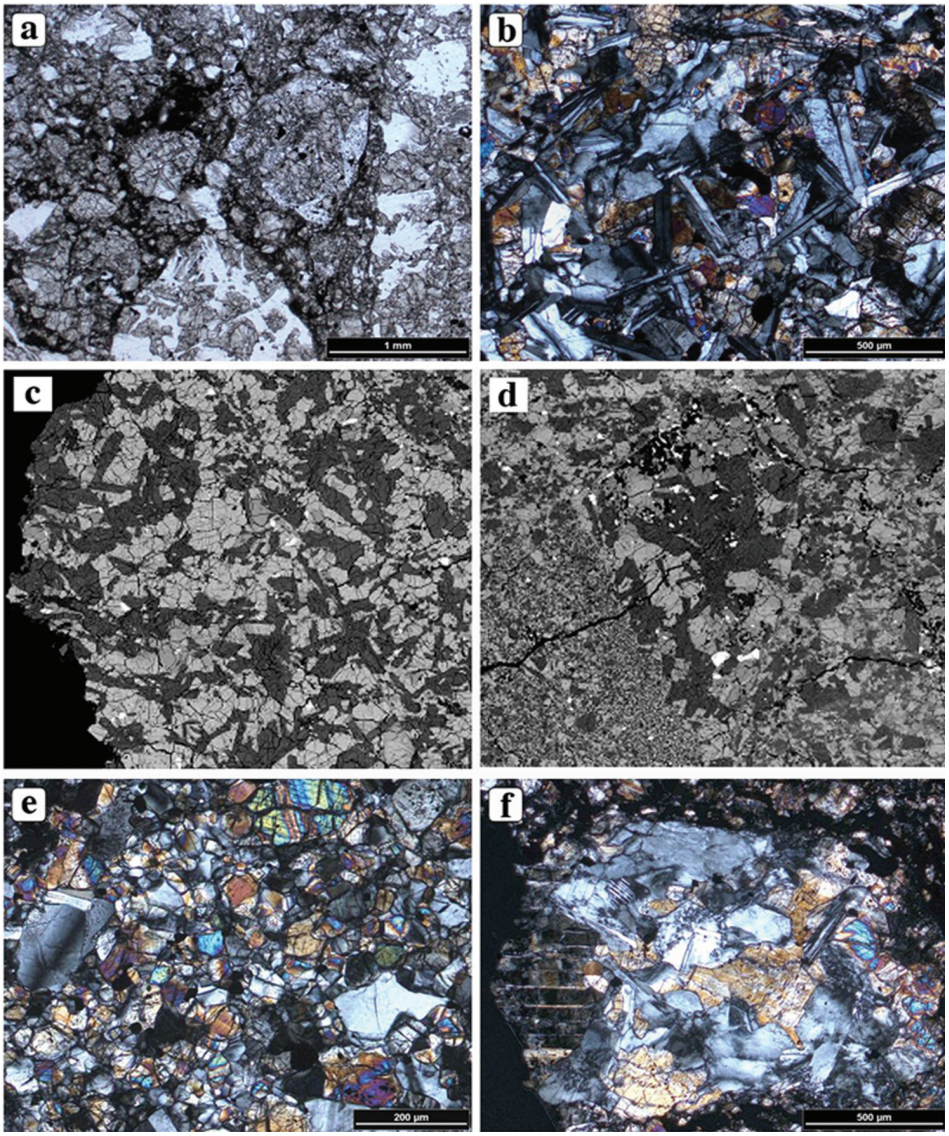

Fig. 3. Photomicrographs of characteristic lithologies within Puerto Lápice. a) Typical appearance of the clastic matrix between larger eucritic fragments (right-hand side, lower center). The dark areas contain some shock-melted materials. Transmitted light, plane polarized light. b) Basaltic lithology with abundant plagioclase laths (grey) and interstitial pyroxene. Transmitted light, crossed polarizers. c) Backscattered electron image of a basaltic clast. d) Basaltic clast with the fine-grained, recrystallized area (left-hand side). Note the textural layering due to grain size variations within the fine-grained portion. BSE-image. e) Granulitic lithology with abundant 120° triple junctions. Transmitted light, crossed polarizers. f) Coarse-grained eucritic lithology with anhedral minerals exceeding a size of 500 µm. Transmitted light, crossed polarizers.

most calcic found in basaltic eucrites ($An_{75–93}$) (Mittlefehldt et al. 1998; Papike 1998), with the exception of Ibitira (An_{95}; Mittlefehldt 2005). The Fe/Mn and Fe/Mg ratios of pyroxenes in Puerto Lápice have also been evaluated, yielding values of 31.4 ± 0.9 and 1.65 ± 0.03, respectively (±1σ counting uncertainties). For low-Ca pyroxene analyses, total uncertainty on the precision can be estimated from the 1σ standard deviation of the mean of ratios, ±1.3%. All clasts were analyzed using the same analytical conditions; the total uncertainty is a good measure for comparing the data sets. These values are well within the compositional ranges of similar pyroxenes in other basaltic eucrites (Fe/Mn from 31.2 to 32.2, and Fe/Mn from 1.57 to 1.73) (Mittlefehldt 2005). Ilmenite, ulvöspinel and Ti-bearing chromite (up to 3.67 wt% TiO_2) are present in minor amounts as dispersed, anhedral grains that can reach a few tens of microns in size.

Shock Effects

The most obvious shock features are (a) the brecciated nature of the rock and (b) the abundant shock veins in various lithologies. For most shocked meteorites the observed shock effects are consistent with a single shock event that affected the whole rock. However, regolith and fragmental breccias

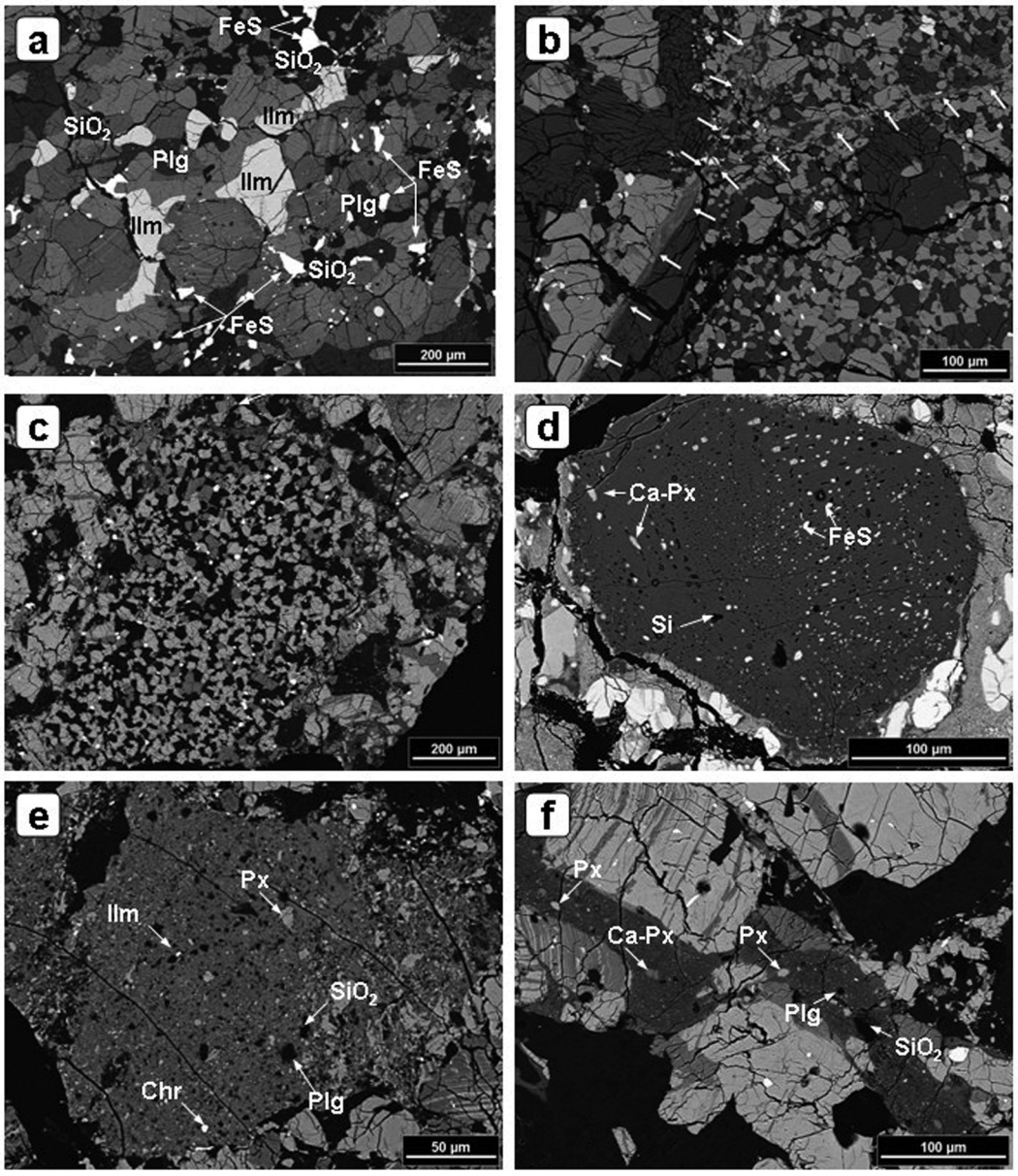

Fig. 4. BSE images of various constituents of the Puerto Lápice eucritic breccia. a) Huge ilmenites (Ilm) and abundant FeS grains (FeS) in paragenesis with pyroxene, plagioclase (Plg), and an SiO_2 phase (SiO_2) within a recrystallized portion of a relatively coarse-grained fragment. The major phase is pyroxene (medium grey with exsolution lamellae). b) Shock vein cutting through the basaltic lithology (left-hand side) and the fine-grained, recrystallized area. c) An individual fine-grained, recrystallized fragment within the clastic matrix. d) Fine-grained clast having abundant tiny inclusions of Ca-rich pyroxene, FeS grains, and lumps of SiO_2-normative materials embedded in an anorthitic plagioclase-normative groundmass. e) Fine-grained breccia-in breccia fragment. f) Shock vein within the clastic matrix of Puerto Lápice. Ca-Px = Ca-pyroxene, Px = low-Ca pyroxene, Si = SiO_2-normative inclusion, Ilm = ilmenite, Chr = chromite, Plg = plagioclase; SiO_2 = SiO_2-phase.

commonly contain clasts of different degree of shock as a result of multiple shock reworking (e.g., Stöffler et al. 1991). Good examples are the lunar regolith and lunar fragmental breccias (e.g., Stöffler et al. 1985; Bischoff et al. 1998). When a shock stage is assigned to such a breccia, a shock pressure experienced by the whole rock is determined (Stöffler et al. 1991). In the Puerto Lápice eucrite, fragments of different shock degree occur. The lowest degree of shock is found within fragments of the basaltic lithology, where plagioclase exhibits undulatory extinction and pyroxene with strong undulose extinction and planar and irregular fractures occurs. Since no planar deformation features in plagioclase are present, the shock stage is S3 according to the stages of shock metamorphism in ordinary and enstatite chondrites (Stöffler et al. 1991; Rubin et al. 1997). Thus, the maximum shock pressure the whole rock may have experienced is about 15 GPa. The shock veins are the result of at least two different shock events. One shock vein type is restricted to the basaltic

Table 1. Average analyses of ilmenite and spinels (chromite and ulvöspinel) in Puerto Lápice. (n = number of different grains analyzed). Bas = basaltic lithology; fine = fine-grained recrystallized areas within the basaltic fragments; IMF = recrystallized impact melt fragments; coarse = coarse-grained eucritic fragments.

	Ilmenite				Chromite		Ulvöspinel
	Fine	Bas	Coarse	IMF	Fine	Bas	Bas
n	4	5	7	1	3	1	2
TiO_2	51.5	53.0	53.0	52.7	2.35	3.67	15.3
Cr_2O_3	0.20	0.14	0.08	0.08	50.9	50.3	33.2
Al_2O_3	0.04	≤0.01	0.03	≤0.01	8.2	8.2	3.5
V_2O_3	n.d.	n.d.	n.d.	n.d.	0.86	0.83	0.58
FeO	45.3	45.1	45.1	44.7	33.5	37.4	44.8
MnO	1.00	0.96	0.95	0.91	0.60	0.67	0.71
MgO	0.53	0.66	0.66	0.52	0.36	0.56	0.44
Sum	98.57	99.87	99.82	98.92	96.77	101.63	98.53
Atoms based on 3 oxygens for ilmenite and 4 oxygens for chromite and ulvöspinel							
Ti	0.9908	1.0011	1.0018	1.0043	0.0651	0.0949	0.4253
Cr	0.0040	0.0027	0.0016	0.0016	1.4838	1.4044	0.9728
Al	0.0013	0.0004	0.0008	0.0003	0.3564	0.3425	0.1534
V					0.0254	0.0235	0.0172
Fe	0.9686	0.9478	0.9480	0.9493	1.0330	1.1051	1.3878
Mn	0.0217	0.0204	0.0202	0.0195	0.0188	0.0201	0.0221
Mg	0.0201	0.0249	0.0246	0.0196	0.0196	0.0295	0.0243
Sum	2.0065	1.9973	1.9970	1.9947	3.0021	3.0199	3.0030

lithology (including the fine-grained recrystallized areas within the basaltic lithology). These shock veins cut through the basaltic and the fine-grained, recrystallized areas (Fig. 4b) and end at the boundary with the clastic breccia matrix. The other shock vein type is almost exclusively restricted to the clastic matrix. These veins are up to about 100 μm thick and represent shock melts (Fig. 4f). Plagioclase close to these areas is frequently transformed to maskelynite indicating shock pressures on the order of 30 GPa (Stöffler et al. 1988, 1991; Bischoff and Stöffler 1992).

MAGNETIC CHARACTERIZATION

For magnetic measurements, three samples of the Puerto Lápice meteorite (LM 1, LM 2, and LM 3) were taken from the interior of separate pieces of the fall (0.10–0.14 g each). Hysteresis loops were run on all samples at 300 K with a SQUID magnetometer. From the hysteresis loops the saturation magnetization, J_S, the remnant saturation magnetization, J_{RS}, the coercive force, H_C, and the remnant coercive force, H_R, were determined (Sugiura and Strangway 1987). The hysteresis loops for all of the Puerto Lápice specimens were very similar. Specific magnetic susceptibility, χ, measured at a low field (0.5 mT) on the three samples gave a logχ of 2.6 ± 0.1 (in 10^{-9} m^3kg^{-1}), typical of other eucrites, 2.8 ± 0.2 (Consolmagno et al. 2006; Smith et al. 2006). These low magnetic susceptibility values are due to depletion in the siderophile elements of eucrites as a result of being the product of partial melting of differentiated parent bodies; eucrites are dominated by Fe-Mg silicates, which are paramagnetic minerals. The $J_{RS}/J_S = 0.1 \pm 0.05$ and $H_c = 5 \pm 0.2$ mT values recorded for Puerto Lápice are higher than average (Sugiura and Strangway 1987), and may correspond to the occurrence of fine-grained Fe metal produced by reduction of silicates, as has been discussed in the preceding section. However, the total metal content of the meteorite calculated from the magnetic susceptibility is low, 1.2 ± 0.2 wt%.

BULK CHEMISTRY

The three samples corresponding to the interior of different specimens of the Puerto Lápice meteorite and used for magnetic characterization were analyzed by wet chemical methods as described elsewhere (Llorca et al. 2007). Two independent methods were used for sample preparation, an acid digestion treatment in a sealed Teflon reactor and an alkaline fusion in a zirconium crucible. Analyses were performed by means of inductively coupled plasma mass spectrometry (ICP-MS) and inductively coupled plasma optical emission spectroscopy (ICP-OES). Results for each independent sample analysis and average composition are compiled in Table 3. From the analysis it can be concluded that Puerto Lápice is very uniform in composition, both in bulk major and trace element composition. This is characteristic of basaltic eucrites.

Fig. 5a is a general plot of CaO versus MgO of HED meteorites (Grossman et al. 1981) showing that Puerto Lápice falls within the basaltic eucrites zone. In a TiO_2 versus mg# (molar MgO/[MgO + FeO]) plot (Fig. 5b), Puerto Lápice

Table 2. Average analyses of representative low- and high-Ca pyroxenes and plagioclase in Puerto Lápice. (n = number of different grains analyzed). Bas = basaltic lithology; fine = fine-grained recrystallized areas within the basaltic fragments; IMF = recrystallized impact melt fragments; coarse = coarse-grained eucritic fragments.

	Fine			Bas			Coarse			IMF		
	Low-Ca	High-Ca	Plag	Low-Ca	High-Ca	Plag	Low-Ca	High-Ca	Plag	Low-Ca	High-Ca	Plag
n	11	6	8	8	8	7	19	12	20	4	4	3
SiO_2	49.3	51.4	45.4	49.4	51.2	45.0	49.2	50.9	46.1	49.7	51.3	45.5
TiO_2	0.09	0.19	0.02	0.14	0.29	0.02	0.14	0.30	0.02	0.12	0.29	0.06
Al_2O_3	0.09	0.41	34.7	0.13	0.43	34.9	0.15	0.47	34.4	0.11	0.45	34.6
Cr_2O_3	0.08	0.23	n.a.	0.09	0.22	n.a.	0.08	0.22	n.a.	0.07	0.24	n.a.
FeO	35.6	16.0	0.50	35.6	16.5	0.40	36.0	16.2	0.18	35.8	16.3	0.46
MnO	1.17	0.56	n.a.	1.13	0.53	n.a.	1.10	0.53	n.a.	1.10	0.54	n.a.
MgO	12.4	10.5	≤0.01	12.2	10.4	≤0.01	12.1	10.3	≤0.01	12.0	10.4	n.d.
CaO	1.32	20.7	18.2	1.56	20.7	18.4	1.24	20.7	18.2	1.09	20.8	18.2
Na_2O	0.02	0.04	0.81	≤0.01	0.05	0.76	0.02	0.05	0.87	0.02	0.06	0.83
K_2O	n.d.	n.d.	0.07	n.d.	n.d.	0.05	n.d.	≤0.01	0.07	≤0.01	n.d.	0.06
Sum	100.07	100.03	99.71	100.26	100.32	99.54	100.03	99.68	99.85	100.02	100.38	99.71
Molar												
Fe/Mn	30.0	28.5		31.1	31.0		32.3	30.4		32.2	29.7	
Fe/Mg	1.61	0.86		1.63	0.89		1.67	0.88		1.67	0.88	
Wo	2.9	43.6		3.4	43.6		2.7	44.0		2.4	43.9	
En	38.1	30.7		37.6	30.6		37.4	30.6		36.8	30.5	
Fs	59.0	25.7		59.0	25.8		59.8	25.4		60.8	25.6	
Ab			7.4			6.9			8.0			8.2
An			92.1			92.7			91.6			91.3
Or			0.4			0.3			0.4			0.5
Atoms per 6 oxygens (pyroxenes) and 8 oxygens (plagioclase)												
Si	1.9781	1.9793	2.1006	1.9768	1.9713	2.0925	1.9769	1.9701	2.1253	1.9898	1.9722	2.1034
Ti	0.0038	0.0073	0.0010	0.0056	0.0111	0.0010	0.0055	0.0116	0.0007	0.0048	0.0113	0.0026
Al	0.0033	0.0140	1.8911	0.0045	0.0146	1.9078	0.0054	0.0161	1.8680	0.0040	0.0152	1.8860
Cr	0.0018	0.0052		0.0022	0.0051		0.0018	0.0051		0.0015	0.0055	
Fe	1.1924	0.5161	0.0195	1.1903	0.5317	0.0196	1.2088	0.5255	0.0069	1.1995	0.5238	0.0178
Mn	0.0397	0.0181		0.0383	0.0171		0.0375	0.0173		0.0372	0.0177	
Mg	0.7386	0.6020	0.0003	0.7290	0.5981	0.0003	0.7235	0.5972	0.0004	0.7181	0.5961	0.0000
Ca	0.0565	0.8544	0.9024	0.0667	0.8526	0.9063	0.0532	0.8579	0.8979	0.0466	0.8576	0.9034
Na	0.0012	0.0027	0.0726	0.0005	0.0038	0.0730	0.0012	0.0038	0.0779	0.0012	0.0043	0.0744
K	0.0000	0.0001	0.0041	0.0001	0.0001	0.0041	0.0001	0.0003	0.0042	0.0003	0.0001	0.0035
Sum	4.0155	3.9992	4.9917	4.0140	4.0055	4.9950	4.0139	4.0049	4.9814	4.0030	4.0037	4.9913

concentrations indicate that the meteorite belongs to the main group of basaltic eucrites. However, the Cr_2O_3 content of this meteorite, 0.46 wt%, is significantly higher than the average value for main group basaltic eucrites (0.30–0.35 wt%). Relative to CI chondrites, the elemental distribution pattern of the Puerto Lápice eucrite is characterized by high concentrations of refractory incompatible lithophile elements. Chalcophiles and particularly siderophiles occur in rather low concentrations. This compositional trend is typical of eucrites (Kitts and Lodders 1998). Also, the concentration of the highly siderophile and chalcophile element molybdenum (50 ppb) and the moderately siderophile element tungsten (160 ppb) is consistent with the constant ratio, independent of absolute concentrations, shown by most eucrites (Newsom 1985).

With respect to the REE, Puerto Lápice displays a flat distribution pattern at about 14 × CI, with no Eu anomaly. This compositional trend typically corresponds to noncumulate eucrites, which are known to display flat distribution patterns at high abundances (~10–20 × CI), whereas cumulate eucrites exhibit diagnostic signatures with significantly lower REE concentrations (~1–5 × CI) and positive Eu anomalies. It is also possible to use the concentrations of incompatible trace elements Sc and La for classifying eucrites (Mittlefehldt et al. 2003; Patzer et al. 2005) (Fig. 5c). Sc is an incompatible element in pyroxene, while La is incompatible in pyroxene and plagioclase. During fractional crystallization of cumulate eucrites, both Sc and La increased in the melt as crystallization proceeded. Model fractional crystallization trends appropriate for eucrite petrogenesis (pigeonite-plagioclase cumulates and residual liquid) are included in Fig. 5c (Stolper 1977; Mittlefehldt and Lindstrom 1993). Puerto Lápice plots with the trace element-poor main group basaltic eucrites and thus could be a primary partial melt.

OXYGEN ISOTOPES

Oxygen isotope analyses were undertaken using an infrared laser fluorination system (Miller et al. 1999). O_2 was liberated by heating the samples using an infrared CO_2 laser

Table 3. Chemical composition of the Puerto Lápice eucrite obtained by wet methods from three different specimens. Uncertainties are 1–5% for all elements except for K (10%).

Major element composition				
wt%	122 mg	109 mg	136 mg	Average
SiO_2	49.2	48.8	49.5	49.19
Al_2O_3	12.6	12.8	13.1	12.84
MgO	7.11	7.08	7.13	7.11
CaO	10.9	10.2	11.1	10.77
Na_2O	0.42	0.37	0.45	0.42
K_2O	0.04	0.03	0.04	0.04
TiO_2	0.81	0.78	0.76	0.78
Cr_2O_3	0.45	0.49	0.44	0.46
MnO	0.53	0.55	0.51	0.53
FeO	17.8	18.3	18.5	18.21
P_2O_5	0.03	0.02	0.02	0.03
S	0.21	0.26	0.18	0.21
Total	100.10	99.68	101.73	

Trace element composition				
µg/g	122 mg	109 mg	136 mg	Average
Sc	30	29	34	31.2
V	81	76	86	81.4
Co	6.3	7.5	5.8	6.5
Ni	15	17	11	14.1
Cu	3.4	5.2	1.7	3.3
Zn	2.1	2.3	1.9	2.1
Ga	1.5	1.8	1.9	1.7
Rb	0.57	0.44	0.43	0.48
Sr	88	95	83	88.2
Mo	0.06	0.04	0.06	0.05
Ba	64	58	69	64.1
Hf	1.7	2.5	2.2	2.1
Ta	0.17	0.16	0.18	0.17
W	0.14	0.17	0.17	0.16
Th	0.37	0.41	0.42	0.40
U	0.13	0.16	0.14	0.14
La	2.3	2.9	2.7	2.6
Ce	10.1	12.4	10.8	11.0
Nd	5.6	4.7	5.2	5.2
Sm	2.3	2.1	1.7	2.0
Eu	0.74	0.65	0.68	0.69
Gd	2.7	2.3	2.1	2.4
Tb	0.6	0.9	0.4	0.61
Dy	3.2	3.6	3.6	3.5
Ho	0.6	0.4	0.3	0.43
Yb	2.7	2.2	2.8	2.6
Lu	0.28	0.48	0.33	0.36

(10.6 µm) in the presence of 210 torr of BrF_5. After fluorination, the O_2 released was purified by passing it through two cryogenic nitrogen traps and over a bed of heated KBr. O_2 was analyzed using a Micromass Prism III dual inlet mass spectrometer. System precision (1σ), based on replicate analyses of international (NBS-28 quartz, UWG-2 garnet) and internal standards, is approximately ±0.04‰ for $\delta^{17}O$; ±0.08‰ for $\delta^{18}O$; ±0.024‰ for $\Delta^{17}O$ (Miller et al. 1999). Oxygen isotope analyses are reported in standard δ notation

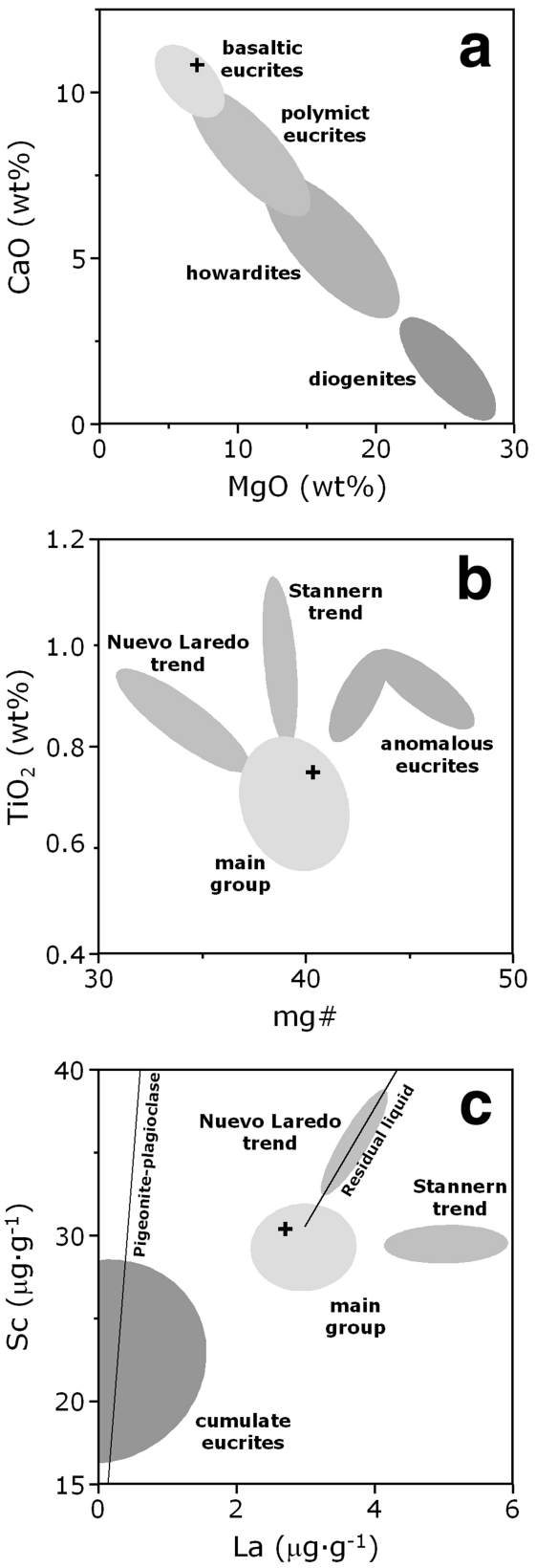

Fig. 5. CaO versus MgO (a), TiO_2 versus mg# (b), and Sc versus La (c) diagrams for HED meteorites, basaltic eucrites, and eucrites, respectively, including Puerto Lápice (+).

Table 4. Helium, neon, and argon abundances and isotopic compositions in Puerto Lápice. Concentrations are in units 10^{-8} cm^3 STP/g, uncertainties in the last digits are given in parentheses. Sample weights were 130.9 mg (LM 2) and 118.4 mg (LM 5), respectively.

Sample	Extr. temp.	^{3}He	^{4}He	^{22}Ne/^{22}Ne	^{20}Ne/^{22}Ne	^{21}Ne/^{22}Ne	^{36}Ar	^{38}Ar/^{36}Ar	^{40}Ar/^{36}Ar
LM 2	600 °C	20.63 (67)	286.4(8.2)	1.365 (34)	0.7180 (37)	0.7793 (51)	0.461 (8)	1.470 (9)	233.6 (1.2)
	1000 °C	1.86 (5)	211.2 (6.1)	1.611 (41)	0.8300 (41)	0.8832 (55)	0.500 (9)	1.503 (10)	981.3 (5.4)
	1800 °C	0.055 (2)	25.8 (8)	1.725 (44)	0.8305 (43)	0.8820 (56)	0.872 (15)	1.511 (10)	190.4 (1.0)
	Total	22.55 (67)	523.4 (10.2)	4.683 (70)	0.7980 (24)	0.8529 (32)	1.833 (19)	1.498 (6)	416.9 (2.3)
LM 5	600 °C	18.84 (55)	146.1 (4.3)	1.828 (47)	0.7446 (37)	0.7834 (49)	0.227 (4)	1.341 (9)	352.2 (1.8)
	1800 °C	1.01 (3)	220.1 (6.4)	2.808 (72)	0.8161 (39)	0.8340 (51)	1.330 (23)	1.510 (10)	619.3 (3.2)
	Total	19.84 (55)	366.2 (7.7)	4.636 (86)	0.7879 (28)	0.8140 (36)	1.557 (24)	1.486 (8)	580.4 (2.8)

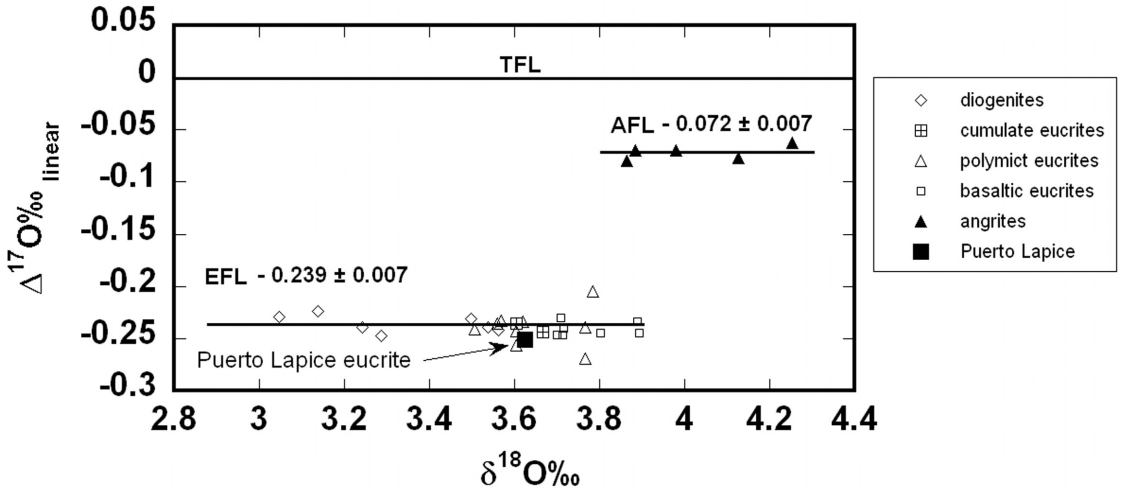

Fig. 6. Oxygen isotopic composition of Puerto Lápice compared to analyses of other HED meteorites (Greenwood et al. 2005). Also shown for reference are the terrestrial fractionation line (TFL) and the angrite fractionation line (AFL) (Greenwood et al. 2005).

where $\delta^{18}O$ has been calculated as: $\delta^{18}O = [(^{18}O/^{16}O_{sample}/^{18}O/^{16}O_{ref})-1] \times 1000$ and similarly for $\delta^{17}O$ using $^{17}O/^{16}O$ ratio. In keeping with other recent oxygen isotope laser fluorination studies of HED samples (Wiechert et al. 2004; Greenwood et al. 2005) $\Delta^{17}O$ is calculated using a linearized format, where $\Delta^{17}O = 1000 \ln [1+ (\Delta^{17}O/1000)]—\lambda 1000 \ln [1+ (\delta^{18}O/1000)]$ where $\lambda = 0.5247$ (Miller 2002).

The results from two replicate analyses of material sampled from the LM 2 specimen of Puerto Lápice are $\delta^{17}O$ = 1.68, 1.62; $\delta^{18}O$ = 3.66, 3.59; and $\Delta^{17}O$ = –0.223, –0.248. The mean value is plotted on Fig. 6 and, for comparison with Puerto Lápice, are the HED oxygen isotope analyses of Greenwood et al. (2005). The mean $\Delta^{17}O_{linear}$ value for Puerto Lápice of –0.251 ± 0.017 (1σ) is within error of the value obtained by Greenwood et al. (2005) for the HED as a whole i.e., –0.239 ± 0.007 (1σ). This indicates that Puerto Lápice is a normal member of the HED suite. Puerto Lápice has a slightly lower $\delta^{18}O$ value than the basaltic eucrites measured by Greenwood et al. (2005). This may reflect a slighter higher orthopyroxene, and/or lower plagioclase content in Puerto Lápice when compared to the basaltic eucrites analyzed by Greenwood et al. (2005). The mean oxygen isotope value for Puerto Lápice falls within the range of values obtained by Greenwood et al. (2005) for both the cumulate eucrites and polymict eucrites (Fig. 6).

NOBLE GAS ANALYSIS

Noble gases have been studied in two specimens, LM 2 (130.9 mg; 3 temperature steps) and LM 5 (118.4 mg; 2 temperature steps) using standard procedures (e.g., Schwenzer et al. 2007). Results for He, Ne, and Ar are listed in Table 4, those for Kr and Xe in Tables 5 and 6. They show patterns typical for eucrites with dominant cosmogenic and radiogenic contributions. There is no evidence for trapped He and Ne. Also Ar is of purely radiogenic and cosmogenic origin, showing evidence neither for trapped Ar nor for contaminating air, as may be expected for a fresh fall. Some trapped or contaminating air Kr and Xe is released at the lowest extraction temperature, however.

Radiogenic and Cosmogenic Gases

After correction for presence of cosmogenic ^{4}He assuming $(^4He/^3He)_{cos} = 4$ (Schwenzer et al. 2007) and all ^{3}He to be of cosmogenic origin, abundances of radiogenic

Table 5. Krypton abundances and isotopic compositions in samples from Puerto Lápice. Concentrations are in units 10^{-12} cm^3 STP/g, uncertainties in the last digits are given in parentheses. Sample weights were 130.9 mg (LM 2) and 118.4 mg (LM 5), respectively.

Sample	Extr. temp.	^{84}Kr	^{78}Kr/^{84}Kr	^{80}Kr/^{84}Kr	^{82}Kr/^{84}Kr	^{83}Kr/^{84}Kr	^{86}Kr/^{84}Kr
LM 2	600 °C	6.08 (47)	0.0368 (43)	0.1295 (91)	0.3254 (81)	0.3542 (129)	0.2730 (97)
	1000 °C	5.49 (39)	0.1483 (80)	0.4595 (229)	0.7327 (295)	0.9539 (407)	0.1535 (105)
	1800 °C	6.97 (39)	0.2194 (114)	0.5712 (215)	0.9850 (363)	1.2299 (455)	0.1647 (134)
	Total	18.54 (73)	0.1385 (52)	0.3933 (114)	0.6940 (170)	0.8611 (222)	0.1987 (68)
LM 5	600 °C	10.51 (56)	0.0139 (30)	0.0691 (52)	0.2538 (64)	0.2652 (99)	0.2939 (130)
	1800 °C	12.13 (48)	0.2098 (62)	0.5660 (216)	0.8751 (203)	1.1525 (327)	0.1607 (85)
	Total	22.65 (73)	0.1188 (40)	0.3353 (126)	0.5866 (125)	0.7405 (197)	0.2226 (77)

Table 6. Xenon abundances and isotopic compositions in samples from Puerto Lápice. Concentrations are in units 10^{-12} cm^3 STP/g, uncertainties in the last digits are given in parentheses. Sample weights were 130.9 mg (LM 2) and 118.4 mg (LM 5), respectively.

Sample	Extr. temp.	^{132}Xe	^{124}Xe/^{132}Xe	^{126}Xe/^{132}Xe	^{128}Xe/^{132}Xe	^{129}Xe/^{132}Xe	^{130}Xe/^{132}Xe	^{131}Xe/^{132}Xe	^{134}Xe/^{132}Xe	^{136}Xe/^{132}Xe
LM 2	600 °C	1.99 (17)	0.0045 (14)	0.0077 (12)	0.0719 (57)	0.9588 (252)	0.1405 (75)	0.7843 (273)	0.3786 (195)	0.3469 (147)
	1000 °C	2.69 (17)	0.0768 (48)	0.1134 (68)	0.2281 (104)	0.9483 (304)	0.1959 (95)	0.9961 (265)	0.4805 (141)	0.4595 (168)
	1800 °C	4.85 (21)	0.0977 (49)	0.1654 (61)	0.2633 (84)	0.6848 (156)	0.2189 (76)	0.9737 (248)	0.6300 (182)	0.6501 (130)
	Total	9.54 (32)	0.0724 (29)	0.1178 (38)	0.2135 (55)	0.8163 (130)	0.1961 (50)	0.9405 (158)	0.5354 (109)	0.5331 (90)
LM 5	600 °C	2.42 (19)	0.0035 (12)	0.0079 (11)	0.0811 (68)	0.9545 (395)	0.1552 (102)	0.8242 (413)	0.3913 (168)	0.3391 (135)
	1800 °C	7.14 (27)	0.0990 (31)	0.1586 (43)	0.2795 (84)	0.7617 (164)	0.2135 (32)	0.8993 (17)	0.6191 (127)	0.6124 (112)
	Total	9.56 (33)	0.0748 (26)	0.1204 (37)	0.2292 (70)	0.8105 (160)	0.1987 (36)	0.8803 (167)	0.5614 (108)	0.5431 (97)

Table 7. Cosmogenic nuclides, shielding parameter $(^{22}Ne/^{21}Ne)_c$, production rates, and resulting ages (following the procedure of Eugster and Michel [1995]) for Puerto Lápice. Gas concentrations are given in units of 10^{-8} cm^3 STP/g for He, Ne, and Ar, 10^{-12} cm^3 STP/g for Kr and Xe. Uncertainties in the last digits are in parentheses. Exposure ages are in Ma, production rates accordingly in 10^{-8} cm^3 STP/(g Ma) (He, Ne, Ar) and 10^{-12} cm^3 STP/(g Ma) (Kr, Xe).

	$(^{22}Ne/^{21}Ne)_c$		$^{3}He_c$	$^{21}Ne_c$	$^{38}Ar_c$	$^{78}Kr_c$	$^{126}Xe_c$
LM 2	1.177 (5)	Concentration	22.5 (7)	3.99 (6)	2.74 (3)	2.49 (13)	1.11 (5)
		Production rate	1.63	0.188	0.159	0.128	0.083
		Age	13.8	21.3	17.2	19.5	13.3
LM 5	1.234 (6)	Concentration	19.8 (5)	3.77 (7)	2.30 (4)	2.49 (13)	1.13 (5)
		Production rate	1.60	0.169	0.159	0.128	0.083
		Age	12.4	22.3	14.5	19.4	13.7

^{4}He are 433 and 287 × 10^{-8} cm^3 STP/g for LM 2 and LM 5, respectively. Taking into account the average Th and U concentrations determined in this work (Table 3), the corresponding U/Th-He gas retention ages are 151 Ma and 100 Ma, indicative of severe recent He losses, as is commonly seen in eucrites (cf. noble gas compilation by Schultz and Franke [2004]). Loss of radiogenic ^{40}Ar is less severe and the nominal K-Ar ages are 2630 and 2860 Ma, based on average K abundance (Table 3) and ^{40}Ar abundances (Table 4).

Abundances of cosmogenic nuclides ^{3}He, ^{21}Ne, ^{38}Ar, ^{78}Kr and ^{126}Xe are listed in Table 7 together with the cosmogenic $(^{22}Ne/^{21}Ne)_{cos}$ ratio, which serves as a shielding parameter for deducing the relevant empirical production rates. Those rates calculated according to the empirical formalism for eucrites of Eugster et al. (1995) and using the average chemical composition in Table 3 are also listed in Table 7 together with the resulting cosmic ray exposure ages. According to $(^{22}Ne/^{21}Ne)_{cos}$ ratios, it is obvious that the LM 5 sample was exposed to cosmic rays in a position much closer to the surface of the meteoroid than the LM 2 sample, which appears to have been irradiated under essentially average (Eugster and Michel 1995) shielding. We have attempted to obtain information on depth profiles using the Leya et al. (2000) predictions for Ne production rates as a function of shielding depth and meteoroid size in the case of eucrites, but such a large difference in $(^{22}Ne/^{21}Ne)_{cos}$ as observed is not predicted to occur between any two positions in a meteoroid of Puerto Lápice composition. One reason may be that the Leya et al. (2000) calculations are aimed at reproducing the situation in chondrites, while in eucrites the abundance of Mg —the element primarily responsible for the variations in the ratio—is much lower.

Among the nominal cosmic ray exposure ages listed in Table 7 we consider T_{21}, T_{38} and T_{78} for LM 2 as the most reliable. LM 2 has more typical shielding, so production rates are probably more reliable than for LM 5. Cosmogenic ^{3}He, as radiogenic ^{4}He, and as often observed in eucrites (Eugster and Michel 1995), shows evidence for diffusion losses, while the abundance of cosmogenic ^{78}Kr is more reliably determined than that of cosmogenic ^{83}Kr. An average age based on ^{21}Ne, ^{38}Ar and ^{78}Kr is 19 ± 2 Ma, hence the Puerto Lápice eucrite may belong to the exposure cluster that has been identified at either 21 ± 4 Ma (Eugster and Michel 1995) or 22 ± 2 Ma (Shukolyukov and Begemann 1996a).

Cosmogenic and Fissiogenic Xenon

In addition to spallation, the Xe isotopic composition is dominated by fission contributions. Data for the heavy isotopes in all temperature steps, after correction for spallation, are plotted in Fig. 7. Figure 7a is a plot of ^{134}Xe/^{132}Xe versus ^{136}Xe/^{132}Xe, where spallation corrections are based on the abundance of spallation ^{126}Xe and assuming spallation Xe to have the isotopic composition deduced by Hohenberg et al. (1981) from data on Angra dos Reis for chondritic target element composition. In partitioning ^{126}Xe the trapped component was assumed to be air, which is not critical, since ^{126}Xe is dominated by spallation (~60% for the 600 °C steps, >98% for the higher temperature releases). Figure 7a clearly shows that the fission component is from ^{244}Pu and that contributions from spontaneous fission of ^{238}U (or from induced fission of ^{235}U) are minor. Abundances of fissiogenic ^{136}Xe in the two specimens are virtually identical at ~3.2 (± 0.3) × 10^{-12} cm^3 STP/g, to which spontaneous fission of ^{238}U (Table 3) should have contributed some 4% over the ~4.5 Ga age of the meteorite. Figure 7b is a plot of ^{131}Xe/^{132}Xe versus ^{136}Xe/^{132}Xe where, in contrast to Fig. 7a, the ratio plotted on the ordinate is sensitive to the correction for cosmogenic Xe, since the production of ^{131}Xe depends critically on shielding due to neutron capture on ^{130}Ba (e.g., Eugster and Michel 1995). The best fit to the mixing line between air and fissiogenic Xe (with 96% Pu and 4% U contribution) is obtained if we choose $(^{131}Xe/^{126}Xe)_{cos}$ as ~3.35 for LM 2 and ~2.6 for LM 5. This is in excellent agreement with what is expected from the ^{22}Ne/^{21}Ne shielding parameter in Table 7 and the relation between the two cosmogenic ratios given in equation 20 of Eugster et al. (1995), from which ~3.7 and ~2.7 would be expected. For comparison, the small open symbols in Fig. 7b show the position of the data points for a choice of $(^{131}Xe/^{126}Xe)_{cos}$ = 3.77 (the value typical for a chondritic Ba/REE ratio as derived from data for Angra dos Reis by Hohenberg et al. 1981).

Our data also allow calculating a Pu-fission Xe age following the procedure of Shukolyukov and Begemann (1996b). The method relies on the geochemical coherence between Pu and light REE and calculates the age by comparing the amounts of fission Xe and cosmogenic Xe (normalized to exposure age). For a cosmic ray exposure age of 19 ± 2 Ma, the resulting Pu-Xe age is 20 ± 19 Ma younger than Angra dos Reis (the reference in the method), which again is quite typical for eucrites (Shukolyukov and Begemann 1996b).

COSMOGENIC RADIONUCLIDES

Three samples of the Puerto Lápice eucrite, i.e., LM 1b, LM 5 and LM 10, have been measured and analyzed by means of non-destructive gamma-ray spectrometry. The measurements were performed using high purity Germanium (HPGe) detectors, in ultra low background configuration (25 cm of lead and an inner liner of 5 cm copper, inside an underground laboratory with 1400 m rock overburden). Two of the specimens (LM 1b and LM 5) were measured rather shortly after the fall (about 55 days), and one (LM 10) significantly later (154 days after the fall). The counting efficiency was determined with a thoroughly tested Monte-Carlo code based on the CERN library GEANT4.

The measured activity concentrations for the detected cosmogenic radionuclides (^{22}Na, ^{54}Mn, ^{7}Be, ^{46}Sc, ^{26}Al) are

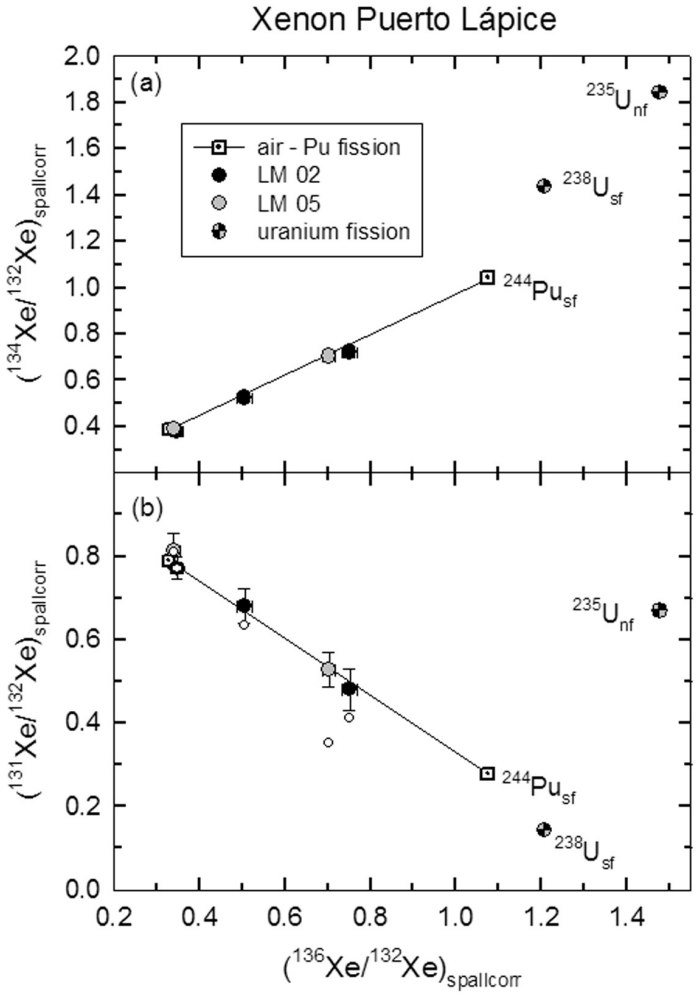

Fig. 7. Three isotope plots for heavy xenon isotopes: $^{134}Xe/^{132}Xe$ versus $^{136}Xe/^{132}Xe$ (a: top) and $^{131}Xe/^{132}Xe$ versus $^{136}Xe/^{132}Xe$ (b: bottom), after correction for cosmogenic contributions. The relative abundance of cosmogenic ^{131}Xe is sensitive to shielding conditions, and a best match is achieved for $(^{131}Xe/^{126}Xe)_c = 3.35$ for LM 2 and 2.6 for LM 5. For comparison, the small open symbols show the position of the data points for a choice of $(^{131}Xe/^{126}Xe)_c = 3.77$ (see text for discussion).

Table 8. Data summary for the detected cosmogenic radionuclides in three samples of the Puerto Lápice eucrite. The reported uncertainties in the last digits (in parentheses) are expanded uncertainties with k =1, the upper limits are given with 90% C.L. The calculated activities are taken from Bhandari et al. (1993).

			Activity concentrations (dpm/kg)		
Radionuclide	Half-life	Calculated activity	LM 1b (5.704 g)	LM 5 (5.60 g)	LM 10 (29.44 g)
^{26}Al	717,000 yr	–	78 (9)	73 (9)	68 (7)
^{60}Co	5.2710 yr	–	<1.6	<4.2	<1.5
^{54}Mn	312.13 d	57	92 (13)	53 (7)	70 (7)
^{22}Na	2.6027 yr	89	38 (5)	39 (5)	42 (4)
^{46}Sc	83.788 d	8.5	9.5 (1.5)	9.5 (2.3)	9.9 (1.3)
^{7}Be	53.22 d	82	378 (206)	238 (50)	223 (46)

given in Table 8. As might be expected from the average composition of the Puerto Lápice eucrite (Table 3), and for eucrites in general, the production of ^{60}Co is negligible. Indeed, only upper limits could be observed. In order to derive an approximate size of the meteorite body the data for the other radionuclides has to be used. The long-lived spallation product ^{26}Al, consistent with the exposure ages derived from the noble gas analyses, has reached its saturation activity, which means that it can also be interpreted as production rate. As reported in literature (Herpers et al. 1990) the production rate for eucrites varies widely between 46 and 122 dpm/kg with an average value of (93 ± 14) dpm/kg (Aylmer et al. 1988). Assuming the ^{26}Al concentration in all three samples to be constant, the average production rate

measured is (72 ± 5) dpm/kg, well in agreement with the above-cited average value. This is consistent with a simple exposure history of the meteoroid. Taking the calculated depth profiles for ^{26}Al production in eucrites from Herpers et al. (1990), this value corresponds to a spherical object of about 10 to 15 cm radius. This is also in good agreement with the radius derived from the calculated depth profile for the production of ^{21}Ne in Herpers et al. (1990) for the values measured (see Table 7) for sample LM 5. Unfortunately, only this sample has been analyzed using both gamma-ray spectrometry and noble gas analysis.

The ^{26}Al activity is representative of the production integrated over a million years or more. The activities of the short-lived radioisotopes, with half-lives less than the orbital period, are instead representing the production integrated over the last segment of the orbit. The fall of the Puerto Lápice eucrite occurred during the solar minimum preceding solar cycle 24. The galactic cosmic ray (GCR) flux was high in the six months before the fall as indicated by the Climax neutron monitor data. This should have increased the activity of the very short lived radionuclides (^{46}Sc and ^{54}Mn). This situation is quite similar to the Piplia Kalan eucrite as reported by Bhandari et al. (1998). Taking the calculations in order to predict the activities for the short-lived radionuclides using the composition of Piplia Kalan as reported in that paper, their activity concentrations are consistent with the expected values calculated on the sun spot numbers as index of GCR activity (Bonino et al. 1995). Our measured values for ^{46}Sc and ^{54}Mn, normalized to their primary targets, are maximal as for the Piplia Kalan eucrites, following the sun spot number.

The values measured for ^{7}Be are three times higher than what is expected from the calculations. This might be due to different shielding. The activity measured for the short lived isotope ^{22}Na is somewhat lower than what is expected. This can be explained arguing that either the size of the meteoroid was, with respect to the Piplia Kalan eucrite, insufficient in order to completely develop the nuclear cascade for the isotope production, or that the three samples that have been analyzed are all coming from a smaller depth. The latter explanation would also be in agreement with the findings of the noble gas analysis of the specimens LM 2 and LM 5, where LM2 seems to come from a greater depth with respect to LM5. The concentrations of the natural radionuclides ^{232}Th and ^{238}U as well as for K_{nat} in the meteorite specimens are listed in Table 9. They are well in accordance with the concentrations obtained by the wet method for these elements as reported in Table 3.

Table 9. Results for the naturally occurring nuclides Th, U, and K_{nat} in three samples of the Puerto Lápice eucrite. The reported uncertainties in the last digits (in parentheses) are expanded uncertainties with k = 1.

	Concentrations (ng/g)		
Nuclide	LM 1b (5.704 g)	LM 5 (5.60 g)	LM 10 (29.44 g)
Th	333 (18)	252 (23)	289 (13)
U	109 (6)	213 (53)	128 (25)
K_{nat}	340 (38) × 10^3	285 (44) × 10^3	264 (28) × 10^3

DISCUSSION

Classification of Puerto Lápice

The Puerto Lápice meteorite has all the signatures characteristic of the main group basaltic eucrites of the HED group. The mineral composition of pyroxenes and plagioclase throughout the different clast types of the meteorite are indistinguishable and well within the compositional ranges in other basaltic eucrites (Mittlefehldt 2005). Consequently, the bulk chemistry of Puerto Lápice is consistent with main group basaltic eucrites (Kitts and Lodders 1998), as it is the specific magnetic susceptibility of the meteorite (Consolmagno et al. 2006; Smith et al. 2006). In addition, oxygen isotopes, which represent an excellent tool for discriminating between HED eucrites and other basaltic achondrites (Greenwood et al. 2005), indicate that Puerto Lápice is a normal member of the HED suite. This is also consistent with the cosmic ray exposure age determined by Ne, Ar, and Kr isotope analysis (19 ± 2 Ma) and the Pu-Xe age calculated from Xe isotopic composition. The Puerto Lápice eucrite exhibits a strong brecciated texture and abundant shock veins. The petrological study of the meteorite reveals that fragments of different shock degree occur, typical of regolith and fragmental breccias, and a shock stage of S3 is evaluated for the whole meteorite. Based on the above, we conclude that the Puerto Lápice meteorite is a basaltic eucrite breccia of the HED group.

Formation of the Puerto Lápice Fragmental Breccia

Puerto Lápice contains various types of clasts embedded in a fragmental, well consolidated matrix. Clast lithologies include basalts (Fig. 3b), in some cases having fine-grained recrystallized melt areas (Fig. 3d), coarse-grained eucritic fragments (Fig. 3f), granulitic materials (Fig. 3e), recrystallized impact melts (Fig. 4c), breccia-in-breccia fragments (Fig. 4e), and fine-grained, anorthite-normative clasts (Fig. 4d). Mineral compositions are very similar throughout the analyzed sections, irrespective of clast lithology, suggesting that all components were equilibrated before lithification. Cooling of a lava flow at the surface of the parent body is unlikely to produce such a homogeneous mineral chemistry; therefore, Puerto Lápice probably represents an annealed sample from depths in the parent body where metamorphic temperatures prevailed to allow phase equilibration by diffusion. Thus, the bulk rock breccia probably derived from the subsurface of a mega-regolith rather than from the direct surface of the parent body and must be defined as a fragmental breccia. The lack of solar wind-implanted gases is also consistent with such a hypothesis of formation.

The formation of breccias like Puerto Lápice requires

mass transport and, therefore, relative movement of rock fragments and their displacement from the primary location in the source material (Stöffler et al. 1988; Bischoff et al. 2006). The presence of recrystallized impact melt lithologies is strongly suggestive of shock-induced melting early in the history of the breccia components. These melts must have been buried to some depth in the mega-regolith in order to achieve their recrystallized microstructure and equilibrated mineral compositions. Then, further impact is necessary to remove these recrystallized rocks—probably together with the granulitic lithologies (Fig. 3e)—from depth and mix them with basaltic materials and breccia-in-breccia clasts that had escaped significant thermal annealing.

After mixing, all clast types became embedded in a fine-grained clastic matrix. The loose surface or near-surface material was consolidated to form the present Puerto Lápice breccia by shock lithification of the clastic debris. Breccias other than impact melt breccias are lithified by impacts that caused limited shock-induced grain boundary melting cementing the rock fragments together (Kieffer 1975; Ashworth and Barber 1976; Bischoff et al. 1983). Ashworth and Barber (1976), and Bischoff et al. (1983) showed that ordinary chondrite regolith breccias experienced shock-induced limited grain-boundary melting. This melt is important for consolidating loose debris into a tough brecciated rock (Bischoff et al. 2006). In Puerto Lápice, there are areas within the clastic matrix that have experienced significant interstitial melting during lithification and subsequent production of shock veins (Fig. 4f). It is well known that shock veins are largely the result of localized stress and temperature concentrations at the interfaces of mineral grains of distinctly different shock impedance (e.g., Stöffler et al. 1991). The most significant feature of shocked porous materials (for example in a parent body regolith or sub-regolith) is the extreme heterogeneity of the shock pressure distribution at the microscale. Pressure "spikes" occur as a transient phenomenon before a certain equilibrium shock pressure is reached. This effect is responsible for the presence of shock effects of extremely different intensity on the scale of the constituent minerals (Stöffler et al. 1988; Bischoff and Stöffler 1992). In the case of Puerto Lápice, this process must have been especially important at the silicate-pore space interfaces (e.g., under loose regolith conditions) and triggered the formation of the interstitial melt veins within the matrix. These high-pressure spikes are also responsible for the local transformation of plagioclase into maskelynite, as observed in the Puerto Lápice matrix close to the shock veins.

Timing of Impact Events and Formation of Shock Veins

Several impact events can be inferred from the study of the nature and textural relationships among clasts in Puerto Lápice. The first identifiable shock event is represented by veins in the basaltic lithologies, including the fine-grained recrystallized areas (Fig. 5b). Since these veins end at the boundary of the clastic breccia matrix, they were most probably formed after the shock event forming the impact melt and before the constituents were lithified to form the present Puerto Lápice breccia. However, it is uncertain whether the impact event that removed the recrystallized rocks from depths and mixed it with other lithologies led to the formation of shock veins. The second type of shock vein is almost exclusively restricted to the clastic matrix (Fig. 4f). The formation of these shock veins is apparently independent of the formation of the veins within the basaltic fragments. We suggest that matrix shock veins are produced by the lithification process that converted the loose subsurface material into a fragmental breccia. We do not know whether the lithification shock event was the same as the event that removed the Puerto Lápice breccia from the parent body. In view of these observations the following impact events that modified the constituents of Puerto Lápice can be inferred: (a) the first impact event produced melt pockets that recrystallized at some depth in the parent body; (b) the second impact event led to the formation of the shock veins within the basalts (including the recrystallized areas); (c) the third impact event removed rocks from depth and mixed these with other rock fragments in a near-surface regolith; (d) a fourth impact event lithified the loose regolith material and formed the Puerto Lápice breccia: (e) finally, a fifth impact event ejected the Puerto Lápice meteoroid from the parent body. As discussed above, it is somewhat uncertain whether the impact events (c) and (e) are individual events or whether the effects were triggered by the shock processes (b) and (d), respectively.

SUMMARY AND CONCLUSIONS

Puerto Lápice is a basaltic eucrite that fell near the town of the same name, in Castilla-La Mancha, Spain, on May 10, 2007. A fireball with an east-to-west trajectory was observed and was accompanied by detonations. About 70 fragments of the meteorite, totaling a mass of approximately 0.5 kg, have been recovered to date.

Four polished sections were prepared for petrographic and mineralogical studies. All of them show a brecciated texture, with fragments embedded in a clearly shock-veined, well consolidated matrix. Clasts include basaltic eucrite fragments, granulitic materials, as well as recrystallized impact melts and breccia-in-breccia lithologies. Silicates are homogeneous in composition throughout the studied sections, irrespective of their grain size or location in the clasts, suggesting that the meteorite probably derived from the subsurface of a megaregolith rather than from the direct surface of the parent body. Major phases identified are low-Ca ($Wo_{3.0}En_{38}Fs_{59}$) and high-Ca ($Wo_{44}En_{31}Fs_{25}$) pyroxenes, and anorthitic plagioclase (An_{92}). Minor amounts of pure silica grains have also been found near the edges of two coarse-grained

fragments. Other phases appear in minor to accessory amounts, and include chromite, ilmenite, ulvöspinel, troilite, and rare Ni-free iron metal. Shock veins in the studied thin sections are abundant, and their textural relationships suggest, at least, three major shock events.

The magnetic susceptibility measured in three samples is close to the typical values for eucrites. The coercive force and saturation magnetization measurements are higher than the average for eucrites and, as suggested by petrographic evidence, may be due to the occurrence of fine-grained Fe metal, probably formed locally by high-temperature reduction of silicate iron. Bulk chemical analyses of three different samples show that, in spite of its brecciated nature, Puerto Lápice has a uniform composition like most basaltic eucrites. However, the Cr content is about 50% higher than the average value for main group basaltic eucrites. Trace element composition is also similar to the trends shown by most eucrites. The flat, unfractionated REE pattern shows that the meteorite is a noncumulate eucrite.

Oxygen isotopic composition, determined from two replicate analyses, is indistinguishable, within error, from the meteorites of the HED suite as a whole. Noble gases show typical eucrite patterns with dominant cosmogenic and radiogenic contributions. The He gas retention ages are indicative of severe recent He losses; loss of radiogenic ^{40}Ar is less pronounced, and two nominal K-Ar ages of 2630 and 2860 Ma have been calculated for the two samples analyzed. The cosmogenic ^{22}Ne/^{21}Ne ratio indicates that one of the samples (LM 5) comes from a location much closer to the surface of the meteoroid than the other (LM 2) which appears to have been irradiated under essentially average shielding. This latter sample, therefore, provides a more reliable cosmic-ray exposure age of 19 ± 2 Ma, from ^{21}Ne, ^{38}Ar and ^{78}Kr contents. Based on such an exposure age, a Pu-Xe age of 20 ± 19 Ma younger than the reference Angra dos Reis can be calculated, again in agreement with common values found for eucrites. Based on the amount of cosmogenic ^{21}Ne and ^{26}Al, the preatmospheric size of Puerto Lápice is calculated to be about 20–30 cm in diameter.

Acknowledgments–We thank Thomas Grau, José Vicente Casado, and Francisco Ocaña for providing samples for analysis and K. Metzler (Münster) for discussions on the formation of the breccia. Siegfried Herrmann performed the noble gas analyses. We acknowledge funding from MEC AYA2007-30476-E (Spain). We thank J. Berkley, C. Floss, S. Schwenzer, and Cyrena Goodrich (Associate Editor) for constructive comments in order to improve the quality of the manuscript.

Editorial Handling—Dr. Cyrena Goodrich

REFERENCES

Ashworth J. R. and Barber D. J. 1976. Lithification of gas-rich meteorites. *Earth and Planetary Science Letters* 30:222–233.

Aylmer D., Herzog G. F., Klein J., and Middleton R. 1988. ^{10}Be and ^{26}Al contents of eucrites: Implications for production rates and exposure ages. *Geochimica et Cosmochimica Acta* 52:1691–1698.

Bhandari N., Mathew K. J., Rao M. N., Herpers U., Bremer K., Vogt S., Wölfli W., Hofmann, H. J., Michel R., Bodemann R., and Lange H.-J. 1993. Depth and size dependence of cosmogenic nuclide production rates in stony meteoroids. *Geochimica et Cosmochimica Acta* 57:2361–2375.

Bhandari N., Murty S. V. S., Suthar K. M., Shukla A. D., Ballabh G. M., Sisodia M. S., and Vaya V. K. 1998. The orbit and exposure history of the Piplia Kalan eucrite. *Meteoritics & Planetary Science* 33:455–461.

Bischoff A. and Stöffler D. 1992. Shock metamorphism as a fundamental process in the evolution of planetary bodies: Information from meteorites. *European Journal of Mineralogy* 4:707–755.

Bischoff A., Rubin A. E., Keil K., and Stöffler D. 1983. Lithification of gas rich chondrite regolith breccias by grain boundary and localized shock melting. *Earth and Planetary Science Letters* 66: 1–10.

Bischoff A., Geiger T., Palme H., Spettel B., Schultz L., Scherer P., Schlüter J., and Lkhamsuren J. 1993. Mineralogy, chemistry, and noble gas contents of Adzhi-Bogdo—an LL3–6 chondritic breccia with L-chondritic and granitoidal clasts. *Meteoritics* 28: 570–578.

Bischoff A., Weber D., Clayton R. N., Faestermann T., Franchi I. A., Herpers U., Knie K., Korschinek G., Kubik P. W., Mayeda T. K., Merchel S., Michel R., Neumann S., Palme H., Pillinger C. T., Schultz L., Sexton A. S., Spettel B., Verchovsky A. B., Weber H. W., Weckwerth G., and Wolf D. 1998. Petrology, chemistry, and isotopic compositions of the lunar highland regolith breccia Dar al Gani 262. *Meteoritics & Planetary Science* 33:1243–1257.

Bischoff A., Scott E. R. D., Metzler K., and Goodrich C. A. 2006. Nature and origins of meteoritic breccias. In *Meteorites and the early solar system II*, edited by Lauretta D. S. and McSween Jr. H. Y. Tucson: The University of Arizona Press. pp. 679–712.

Bonino G., Castagnoli G. C., Bhandari N., and Taricco C. 1995. Behavior of the heliosphere over prolonged solar quiet periods by Ti-44 measurements in meteorites. *Science* 270:1648–1650.

Consolmagno G. J., Macke R. J., Rochette P., Britt D. T., and Gattacceca J. 2006. Density, magnetic susceptibility, and the characterization of ordinary chondrite falls and showers. *Meteoritics & Planetary Science* 41:331–342.

Drake M. J. 2001. The eucrite/Vesta story. *Meteoritics & Planetary Science* 36:501–513.

Eugster O. and Michel Th. 1995. Common asteroid break-up events of eucrites, diogenites, and howardites and cosmic-ray production rates for noble gases in achondrites. *Geochimica et Cosmochimica Acta* 59:177–199.

Floss C., Taylor L. A., Promprated P., and Rumble III D. 2005. Northwest Africa 011: A "eucritic" basalt from a non-eucrite parent body. *Meteoritics & Planetary Science* 40:343–360.

Greenwood R. C., Franchi I. A., Jambon A., and Buchanan P. C. 2005. Widespread magma oceans on asteroidal bodies in the early solar system. *Nature* 435:916–918.

Grossman L., Olsen E., Davis A. M., Tanaka T., and MacPherson G. J. 1981. The Antarctic achondrite ALHA76005: A polymict eucrite. *Geochimica et Cosmochimica Acta* 45:1267–1279.

Herpers U., Vogt S., Bremer K., Hofmann H. J., Wölfli W., Bobe K., Stöffler D., Wieler R., Signer P., Michel R., Dragovitsch P., and Filges D. 1990. Cosmogenic nuclides in eucrites. *Nuclear Instruments and Methods in Physics Research B* 52:612–617.

Hohenberg C. M., Hudson B., Kennedy B. M., and Podosek F. A. 1981. Xenon spallation systematics in Angra dos Reis. *Geochimica et Cosmochimica Acta* 45:1909–1915.

Kieffer S. W. 1975. From regolith to rock by shock. *The Moon* 13: 301–320.

Kitts K. and Lodders K. 1998. Survey and evaluation of eucrite bulk compositions. *Meteoritics & Planetary Science* 33:A197–A213.

Leya I., Lange H.-J., Neumann S., Wieler R., and Michel R. 2000. The production of cosmogenic nuclides in stony meteoroids by galactic cosmic-ray particles. *Meteoritics & Planetary Science* 35:259–286.

Llorca J., Trigo-Rodríguez J. M., Ortiz J. L., Docobo J. A., García-Guinea J., Castro-Tirado A. J., Rubin A. E., Eugster O., Edwards W., Laubenstein M., and Casanova I. 2005. The Villalbeto de la Peña meteorite fall: I. Fireball energy, meteorite recovery, strewn field, and petrography. *Meteoritics & Planetary Science* 40:795–804.

Llorca J., Gich M., and Molins E. 2007. The Villalbeto de la Peña meteorite fall: III. Bulk chemistry, porosity, magnetic properties, Fe^{57} Mössbauer spectroscopy, and Raman spectroscopy. *Meteoritics & Planetary Science* 42:A177–A182.

Metzler K., Bobe K.-D., Palme H, Spettel B., and Stöffler D. 1995. Thermal and impact metamorphism on the HED parent asteroid. *Planetary and Space Science* 43:499–525.

Miller M. F. 2002. Isotopic fractionation and the quantification of ^{17}O anomalies in the oxygen three-isotope system: An appraisal and geochemical significance. *Geochimica et Cosmochimica Acta* 66:1881–1889.

Miller M. F., Franchi I. A., Sexton A. S., and Pillinger C. T. 1999. High precision $\Delta^{17}O$ measurements of oxygen from silicates and other oxides: Method and applications. *Rapid Communications in Mass Spectrometry* 13:1211–1217.

Mittlefehldt D. W. 2005. Ibitira: A basaltic achondrite from a distinct parent asteroid and implications for the Dawn mission. *Meteoritics & Planetary Science* 40:665–677.

Mittlefehldt D. W. and Lindstrom M. M. 1993. Geochemistry and petrology of a suite of ten Yamato HED meteorites. *Proceedings of the NIPR Symposium on Antarctic Meteorites* 6:268–292.

Mittlefehldt D. W. and Lindstrom M. M. 2003. Geochemistry of eucrites: Genesis of basaltic eucrites, and Hf and Ta as petrogenetic indicators for altered Antarctic meteorites. *Geochimica et Cosmochimica Acta* 67:1911–1935.

Mittlefehldt D. W., McCoy T. J., Goodrich C. A., and Kracher A. 1998. Non-chondritic meteorites from asteroidal bodies. In *Planetary materials*, edited by Papike J. J. Washington, D.C.: Mineralogical Society of America. pp. 4-1–4-195.

Newsom H. E. 1985. Molybdenum in eucrites: Evidence for a metal core in the eucrite parent body. *Journal of Geophysical Research* 90:C613–C617.

Papike J. J. 1998. Comparative planetary mineralogy: Chemistry of melt-derived pyroxene, feldspar, and olivine. In *Planetary materials*, edited by Papike J. J. Washington, D.C.: Mineralogical Society of America. pp. 7-1–7-11.

Patzer A., Schlüter J., Schultz L., Hill D. H., and Boynton W. V. 2005. The new polymict eucrite Dar al Gani 983: Petrography, chemical composition, noble gas record, and evolution. *Meteoritics & Planetary Science* 40:869–879.

Pun A., Keil K., Taylor G. J., and Wieler R. 1998. The Kapoeta howardite: Implications for the regolith evolution of the howardite-eucrite-diogenite parent body. *Meteoritics & Planetary Science* 33:835–851.

Rubin A. E., Scott E. R. D., and Keil K. 1997. Shock metamorphism of enstatite chondrites. *Geochimica et Cosmochimica Acta* 61: 847–858.

Russell C. T., Coradini A., Christensen U., De Sanctis M. C., Feldman, W. C., Jaumann R., Keller H. U., Konopliv A. S., McCord T. B., McFadden L. A., McSween H. Y., Mottola S., Neukum G., Pieters C. M., Prettyman T. H., Raymond C. A., Smith D. E., Sykes M. V., Williams B. G., Wise J., and Zuber M. T. 2004. Dawn: A journey in space and time. *Planetary and Space Science* 52:465–489.

Schultz L. and Franke L. 2004. Helium, neon, and argon in meteorites. A data collection. *Meteoritics & Planetary Science* 39:1889–1890.

Schwenzer S. P., Herrmann S., Mohapatra R. K., and Ott U. 2007. Noble gases in mineral separates from three shergottites: Shergotty, Zagami, and EETA79001. *Meteoritics & Planetary Science* 42:387–412.

Shukolyukov A. and Begemann F. 1996a. Cosmogenic and fissiogenic noble gases and ^{81}Kr-Kr exposure age clusters of eucrites. *Meteoritics & Planetary Science* 31:60–72.

Shukolyukov A. and Begemann F. 1996b. Pu-Xe dating of eucrites. *Geochimica et Cosmochimica Acta* 60:2453–2471.

Smith D. L., Ernst R. E., Samson C., and Herd R. 2006. Stony meteorite characterization by non-destructive measurement of magnetic properties. *Meteoritics & Planetary Science* 41:355–373.

Stöffler D., Bischoff A., Borchardt R., Burghele A., Deutsch A., Jessberger E. K., Ostertag R., Palme H., Spettel B., Reimold W. U., Wacker R., and Wänke H. 1985. Composition and evolution of the lunar crust in the Descartes highlands, Apollo 16. Proceedings, 15th Lunar and Planetary Science Conference. *Journal of Geophysical Research* 90:C449 C506.

Stöffler D., Bischoff A., Buchwald V., and Rubin A. 1988. Shock effects in meteorites. In *Meteorites and the early solar system*, edited by Kerridge J. and Matthews M. S. Tucson: The University of Arizona Press. pp. 165–202.

Stöffler D., Keil K., and Scott E. R. D. 1991. Shock metamorphism of ordinary chondrites. *Geochimica et Cosmochimica Acta* 55: 3845–3867.

Stolper E. 1977. Experimental petrology of eucrite meteorites. *Geochimica et Cosmochimica Acta* 41:587–611.

Sugiura N. and Strangway D. W. 1987. Magnetic studies of meteorites. In *Meteorites and the early solar system*, edited by Kerridge J. and Matthews M. S. Tucson: The University of Arizona Press. pp. 595–615.

Trigo-Rodríguez J. M., Borovička J., Spurný P., Ortiz J. L., Docobo J. A., Castro-Tirado A. J., and Llorca J. 2006. The Villalbeto de la Peña meteorite fall: II. Determination of the atmospheric trajectory and orbit. *Meteoritics & Planetary Science* 41:505–517.

Trigo-Rodríguez J. M., Borovička J., Llorca J., Madiedo J. M., Zamorano J., Izquierdo J. and 2009. Puerto Lápice eucrite fall: Strewn field, physical description, probable fireball trajectory, and orbit. *Meteoritics & Planetary Science* 44. This issue.

Wiechert U. H., Halliday A. N., Palme H., and Rumble D. 2004. Oxygen isotope evidence for rapid mixing of the HED meteorite parent body. *Earth and Planetary Science Letters* 221:373–382.

Yamaguchi A., Taylor G. J., and Keil K. 1997. Shock and thermal history of equilibrated eucrites from Antarctica. *Antarctic Meteorite Research* 10:415–436.

Yamaguchi A., Clayton R. N., Mayeda T. K., Ebihara M., Oura Y., Miura Y. N., Haramura H., Misawa K., Kojima H., and Nagao K. 2002. A new source of basaltic meteorites inferred from Northwest Africa 011. *Science* 12:334–336.